Journal of Hydrology 513 (2014) 154–163

Contents lists available at ScienceDirect

Journal of Hydrology

journal homepage: www.elsevier.com/locate/jhydrol

The dependence of precipitation types on surface elevation and meteorological conditions and its parameterization

Baohong Ding [a,b,*], Kun Yang [a], Jun Qin [a], Lei Wang [a], Yingying Chen [a], Xiaobo He [c]

[a] Key Laboratory of Tibetan Environment Changes and Land Surface Processes, Institute of Tibetan Plateau Research, Chinese Academy of Sciences, Beijing 100101, China
[b] University of Chinese Academy of Sciences, Beijing 100049, China
[c] State Key Laboratory of Cryospheric Sciences, Cold and Arid Regions Environmental and Engineering Research Institute, Chinese Academy of Sciences, Lanzhou 730000, China

ARTICLE INFO

Article history:
Received 22 October 2013
Received in revised form 12 March 2014
Accepted 15 March 2014
Available online 29 March 2014
This manuscript was handled by
Konstantine P. Georgakakos, Editor-in-Chief

Keywords:
Precipitation type
Wet-bulb temperature
Elevation
Relative humidity
Threshold temperature

SUMMARY

Precipitation types (rain, snow, and sleet) have great impacts on the surface runoff and energy balance. However, many weather stations only record precipitation amount without discriminating its type. Based on CMA (China Meteorological Administration) station data over 30 years, this study investigates the relationship of precipitation types with surface elevation and meteorological variables. Major findings are (1) wet-bulb temperature is a better indicator than air temperature for discriminating precipitation types; (2) precipitation types are highly dependent on surface elevation, and a higher threshold temperature is needed for differentiating snow and rain over a higher-elevation region; and (3) precipitation types are also dependent on relative humidity, and the probability of sleet event rises greatly with the increase of relative humidity. Based on these findings, a new parameterization scheme is developed to determine the precipitation type, with input of daily mean wet-bulb temperature, relative humidity, and surface elevation. Evaluations for China territory show that the new scheme gives better accuracy than 11 other schemes that are used in hydrological and land surface models.

1. Introduction

Precipitation is one of the most important components in water and energy cycle, and the precipitation types (rain, snow, and sleet) have great impacts on the land surface mass and energy balance (Loth et al., 1993). Snowfall can accumulate at the land surface while rainfall usually infiltrates into soils and converges into rivers or groundwater (Clark et al., 2006). The surface albedo increases greatly when snowfall occurs, which can substantially alter the surface energy budget, whereas the effect is opposite when rainfall occurs (Box et al., 2012). Besides, precipitation type is needed for the correction of precipitation gauge data, as the catch ratio of precipitation gauges depends on precipitation type (Yang et al., 1988, 1995; Rasmussen et al., 2012). Therefore, the differentiation of precipitation types is important for land hydrological process studies (Anderson and Mackintosh, 2012).

However, precipitation types are often not observed or not accessible. For example, the data of precipitation amount at more than 700 CMA (China Meteorological Administration) weather stations since 1950s can be obtained via the CMA National Meteorological Information Center (NMIC), but the data of precipitation types is not available for the years after 1979 (Han et al., 2010). So the discrimination of the precipitation types for the recent three decades mainly relies on empirical or semi-empirical relationships derived from other observations. Generally, the discrimination schemes are categorized into two classes according to the used variables.

One class is based on the temperature profile and other atmospheric conditions (e.g. Bocchieri, 1980; Ryzhkov and Zrnic, 1998; Rauber et al., 2001; Lundquist et al., 2008). Czys et al. (1996) presented a non-dimensional parameter (i.e. the ratio of the available time for melting to the required time for complete melting) to differentiate between freezing rain and ice pellets by using air temperature profile. Bourgouin (2000) used the area between the air temperature profile and the 0 °C isotherm on aerological diagrams to diagnose precipitation types. Schuur et al. (2012) employed the vertical profile of wet-bulb temperature derived from the rapid update cycle model (Benjamin et al., 2000) and polarimetric radar retrievals to classify the precipitation types. A challenging issue that hinders the applications of the above schemes is that air temperature profile is generally not available at weather stations.

* Corresponding author at: Institute of Tibetan Plateau Research, Chinese Academy of Sciences, Bldg. 3, Courtyard 16, Lincui Rd., Chaoyang District, Beijing 100101, China. Tel.: +86 10 84097094; fax: +86 10 84097079.
E-mail address: dingbh@itpcas.ac.cn (B. Ding).

http://dx.doi.org/10.1016/j.jhydrol.2014.03.038
0022-1694/

The other class of empirical schemes mainly employs surface air conditions. Their inputs are accessible and thus they are widely used for hydrological and land surface modeling. Among them, surface air temperature-based methods are most widely used for the identification of precipitation types (e.g. Auer, 1974; Kang et al., 1999; Gustafsson et al., 2001), including single threshold methods (Yang et al., 1997; Clark et al., 2006) and dual-threshold methods (Kang, 1994; Wigmosta et al., 1994; Chen et al., 2008). A single threshold method differentiates rain and snow with only one critical temperature. A dual-threshold method uses two critical temperatures to differentiate rain, snow, and sleet: rain occurs when air temperature is higher than an upper critical temperature; snow occurs when air temperature is lower than a lower critical temperature; sleet (as a mixture of rain and snow) occurs when air temperature is between the two critical temperatures. In addition, some schemes are developed to calculate the ratio of snow (or rain) amount to total precipitation amount (Zhang et al., 2013), instead of determining the precipitation type. Yamazaki (2001) used a scheme with the wet-bulb temperature as an indicator to calculate the ratio of snow amount to total precipitation amount for modeling land surface processes in Eastern Siberia. Dai (2008) proposed a method to calculate the frequencies of rain, sleet, and snow from their relationships with both surface air temperature and pressure over land and ocean. Table 1 shows the critical temperatures of nine schemes in the literature and the calculations of snow ratio of the above two schemes; clearly, the critical temperature values are not unique in different regions, and all these schemes need validations for different climate regimes. Particularly, we have little knowledge on how elevations impact the precipitation types.

This study aims at developing a new scheme to discriminate precipitation types, based on more than 400,000 samples of precipitation types collected from different climate regimes and elevations in China. The remaining parts of this paper are organized as follows. Section 2 introduces the dataset and the data quality control procedures. Section 3 presents the dependence of precipitation types on surface wet-bulb temperature, relative humidity, and elevation. Based on their relationships, a new parameterization scheme is developed in Section 4 and its evaluation is presented in Section 5 by comparisons with 11 schemes in the literature. The results are summarized in Section 6.

2. Data

The dataset used in this study is the Version 3.0 of "Daily Surface Climate Variables of China", which is provided by CMA NMIC. This dataset covers the period from 1951 to 1979, with precipitation type information available at daily scale. Therefore, daily weather data are used in this study, including daily mean air temperature (T_a), daily mean relative humidity (RH), daily mean surface pressure (p_s), daily total precipitation (P_r), and precipitation type of 824 stations. Elevation (Z) is also used so as to understand its role in the formation of precipitation.

Generally, the precipitation type is recorded as one of three types (rain, sleet, and snow). Although the data quality has been preliminary controlled by the data provider, some stations recorded all precipitation events as rain throughout all years or some years, without discriminating precipitation types. In addition, erroneous or suspected classifications occur occasionally, since the precipitation type is based on manual judgment and recording. Therefore, the following data quality control procedures are adopted to remove erroneous and suspicious data.

(1) Select qualified data according to the original quality control flag in the dataset. Herein, data are selected if the quality control flags of T_a, RH, p_s, and P_r are simultaneously marked as correct.
(2) Search for erroneous and suspicious data records. A data record is regarded as abnormal if rain occurs when $T_a < 0$ °C, snow occurs when $T_a > 8$ °C, or sleet occurs when $T_a < -1.6$ °C or $T_a > 9.6$ °C, according to statistical results of the precipitation types; otherwise, the data record is regarded as a normal one. Then, we counted for each year of each station (i) the numbers of all samples of rain, snow, and sleet, recorded as N_{rain}, N_{snow}, and N_{sleet}, respectively; and (ii) the numbers of all abnormal samples of rain, snow, and sleet, recorded as $N_{rain,wrong}$, $N_{snow,wrong}$, and $N_{sleet,wrong}$, respectively.

Table 1
Nine schemes of discriminating precipitation-type and two schemes of calculating snow ratio to total precipitation in the literature.

Scheme	Thresholds of T_a or snow ratio	Model	Region and period being applied
Y97 (Yang et al., 1997)	2.2 °C	BATS model	Yershov, Uralsk, Ogurtsovo, Kostroma, Khabarovsk and Tulun (48°N–57°N, 41°E–135°E), 1978–1983
L93 (Loth et al., 1993)	−1 °C, 4 °C	Snow cover model	German meteorological station Potsdam (52°23′, 13°04′), 1975–1980
W94 (Wigmosta et al., 1994)	−1.1 °C, 3.3 °C	DHSVM model	Middle Fork Flathead River basin in northwestern Montana (114°00′W, 48°29′N, 900 m–3000 m), Oct 1988–Oct 1991
K94 (Kang, 1994)	2.8 °C, 5.5 °C	Energy, water, mass balance and hydrological discharge model	Tianshan Mountain, China (43°06′N, 86°50′E, 3539 m–4010 m), 1986–1990
L97 (Lindström et al., 1997)	−1 °C, 1 °C	HBV model	Ten basins in Sweden, 1969–1989
C04 (Collins et al., 2004)	−5 °C, 0 °C	NCAR CAM3.0	
HH05 (Hock and Holmgren, 2005)	0.5 °C, 2.5 °C	Mass balance model	Storglaciären, Sweden (67°55′N, 18°35′E, 1120 m–1730 m), 1993–1994
G10 (Gao et al., 2010)	−0.5 °C, 2 °C	Degree-day mass balance model	Tarim River Basin, China (35°N–43°N, 73°E–93°E, 2780 m–4800 m), 1961–2006
W11 (Wang et al., 2011)	0 °C, 2 °C	Degree-day mass balance model	Qiyi Glacier in Qilian Mountains, China (39.5°N, 97.5°E, 4304 m–5158.8 m), Jun 30–Sep 5, 2010
Y01 (Yamazaki, 2001)	Snow ratio dependent on T_w	One dimensional land surface model	Lena River basin in Eastern Siberia, 1986–1994
D08 (Dai, 2008)	Snow ratio dependent on T_a and p_s		15,000 land stations global and many ships, 1977–2007

(3) Search for abnormal years of each station. For each station, a year is regarded as abnormal if any of the following three conditions happens: (i) $\frac{N_{rain,wrong}}{N_{rain}} \geqslant 10\%$, (ii) $\frac{N_{snow,wrong}}{N_{snow}} \geqslant 30\%$, or (iii) $\frac{N_{sleet,wrong}}{N_{sleet}} \geqslant 30\%$. Then, we counted for each station (i) the number of years in which at least one precipitation type occurs, recorded as Y_{rain}, Y_{snow}, and Y_{sleet}, respectively; and (ii) the number of abnormal years for each type, recorded as $Y_{rain,wrong}$, $Y_{snow,wrong}$, and $Y_{sleet,wrong}$.

(4) Search for abnormal stations. A station is regarded as abnormal if any of the following four conditions happens: (i) $\frac{Y_{rain,wrong}}{Y_{rain}} \geqslant 50\%$, (ii) $\frac{Y_{snow,wrong}}{Y_{snow}} \geqslant 50\%$, (iii) $\frac{Y_{sleet,wrong}}{Y_{sleet}} \geqslant 50\%$, or (iv) $Y_{snow} + Y_{sleet} = 0$.

(5) Remove abnormal data found in Step (2–4). Firstly, remove all data from abnormal stations. Secondly, remove all data from abnormal years for each station. Thirdly, remove all abnormal data records that still remain after the preceding steps.

After all the above quality control steps, the data records with $-10\ ^\circ\mathrm{C} < T_a < 10\ ^\circ\mathrm{C}$ are selected, because this temperature range is concerned in terms of precipitation type discrimination.

The sample size of the precipitation data after the quality control is 459766 collected at 709 stations. The station distribution is shown in Fig. 1. All these stations are separated into a calibration (or analysis) group and a validation group. The calibration group includes 609 stations (containing about 85% of all data) and is used for both the analysis of factors controlling the precipitation types and the development of a new discrimination scheme. The validation group includes 100 stations (containing about 15% of all data) and is used for the validation of the new scheme. These calibration stations are selected randomly with consideration of spatial homogeneity. To test the performance of the scheme in different regions, all the stations are separated into four sub-regions: the Tibetan Plateau, Northwest China, Northeast China and the rest of China. The ratio of the calibration stations to the validation stations is similar in each sub-region.

Fig. 2 shows the sample distribution of rain, sleet, and snow within the calibration group with respect to elevation, relative humidity, air temperature, and wet-bulb temperature. The validation group has a similar distribution as in Fig. 2, with about 14–20% of the samples in each bin.

3. Factors controlling precipitation types

3.1. Dependence on daily mean wet-bulb temperature (T_w)

T_w contains air temperature, humidity, and pressure information, and its calculation is given in the Appendix A. Since precipitating droplets (including rain, sleet, and snow) have a temperature closer to T_w than to air temperature (T_a), it is expected that T_w is more suitable than T_a for indicating the precipitation type. This is also suggested in Fig. 2c and d.

According to Fig. 2c, 99.5% of rain samples occur when $T_a \geqslant 0.5\ ^\circ\mathrm{C}$, and 98.7% of snow samples occur when $T_a \leqslant 5\ ^\circ\mathrm{C}$. In the overlapping range of T_a [0.5 °C, 5 °C], there are 60,799 rain samples, 22,360 snow samples, and 27,222 sleet samples. However, according to Fig. 2d, 99.3% of rain samples occur when $T_w \geqslant -0.7\ ^\circ\mathrm{C}$, and 99% of snow samples occur when $T_w \leqslant 2.5\ ^\circ\mathrm{C}$. In the overlapping range of T_w [−0.7 °C, 2.5 °C], there are 31,600 rain samples, 20,520 snow samples, and 24,258 sleet samples. So, the number of rain samples and snow samples in the overlapping range in terms of T_w is much less than that in terms of T_a. In other words, it is reasonable to use T_w instead of T_a to discriminate precipitation types, as has been suggested by Yamazaki (2001).

To quantify the dependence of the occurrence frequency of each precipitation type on T_w, the precipitation samples for snow, sleet, and rain are counted, respectively, for each 0.2 °C bin of T_w. Fig. 3 shows the ratio of rain, sleet, and snow samples to their total in each bin with dark grey, white, and light grey, respectively. This ratio may be regarded as the probability of the occurrence of each type. As expected, with the increase of T_w, the probability of snowfall deceases, the probability of rainfall

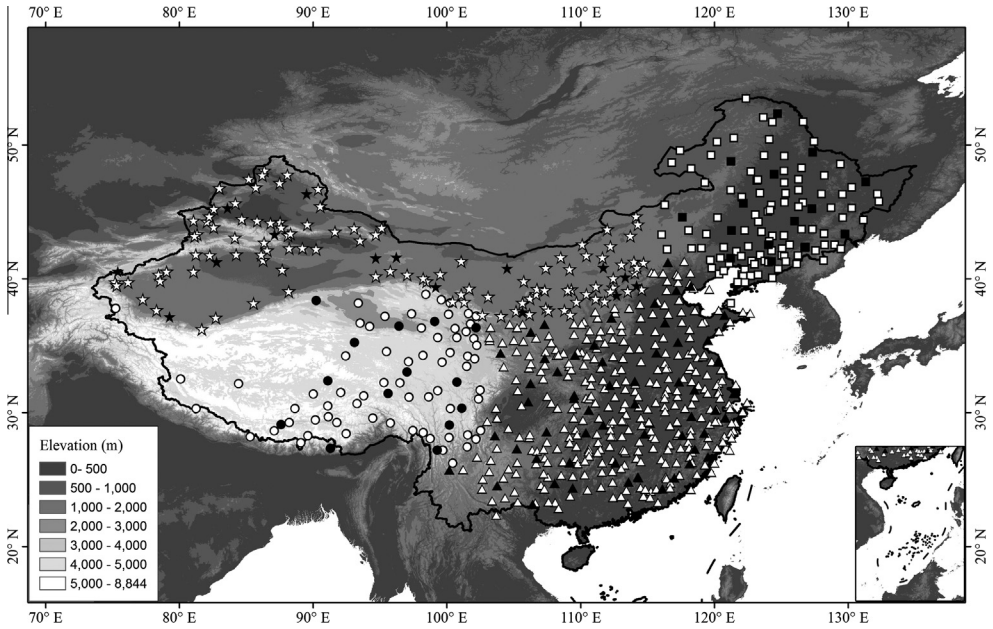

Fig. 1. The distribution of the selected 709 CMA meteorological stations in China. The white marks represent the calibration group that comprises 609 stations for data analysis and scheme development, and the black ones represent the 100 stations for scheme validation. All the stations are separated into four sub-regions: the Tibetan Plateau (round), Northwest China (pentagram), Northeast China (square) and the rest of China (triangle).

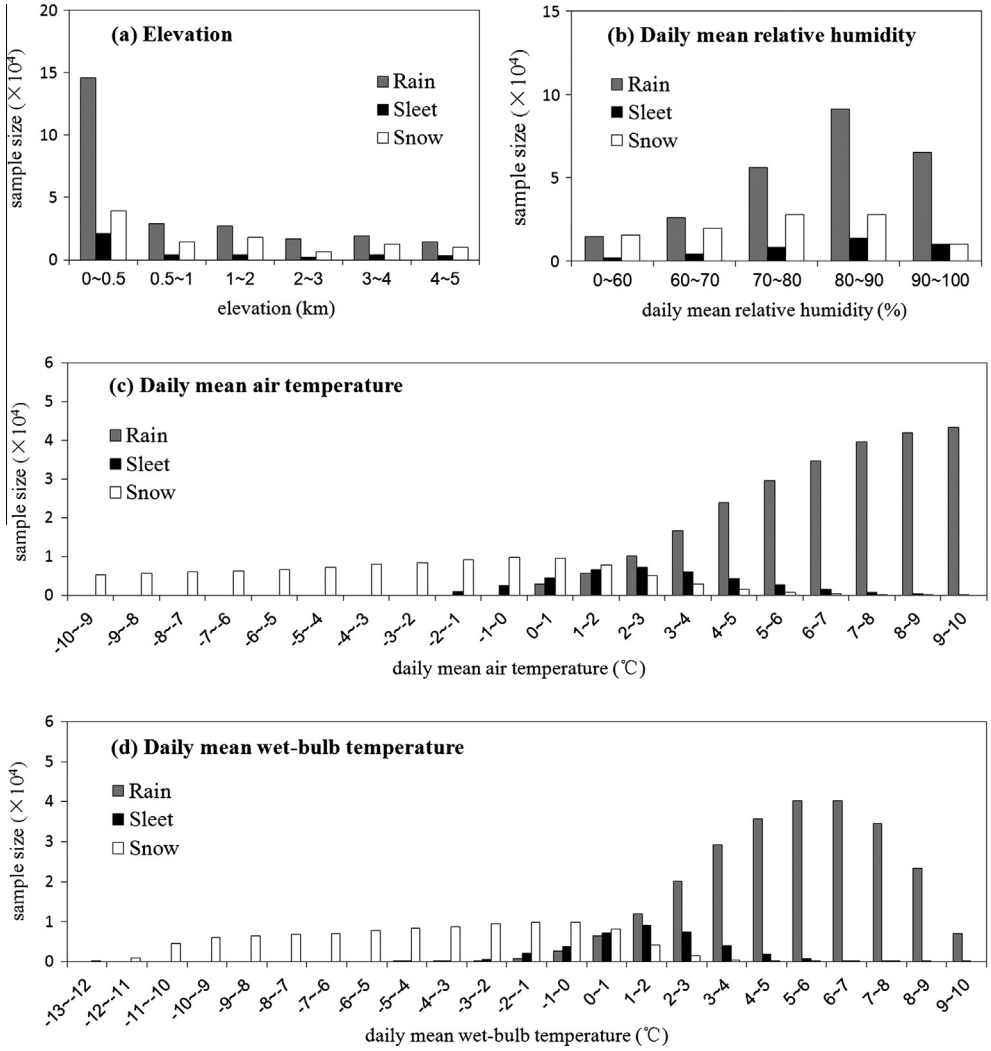

Fig. 2. Sample size distribution of rain, sleet, and snow with respect to (a) elevation, (b) daily mean relative humidity, (c) daily mean air temperature, and (d) daily mean wet-bulb temperature according to the calibration data.

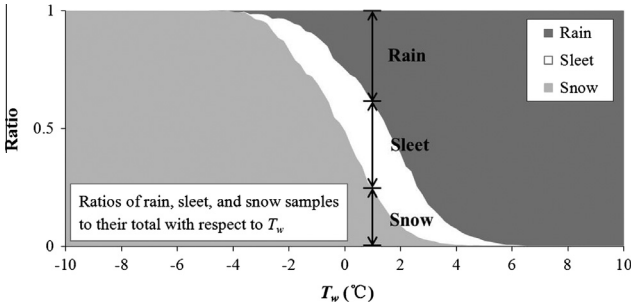

Fig. 3. The individual ratios of rain, sleet, and snow samples to their total with respect to daily mean wet-bulb temperature (T_w) according to the calibration data. The dark grey, white, and light grey represent rain, sleet, and snow, respectively.

increases, and the probability of sleet occurrence first increases and then decreases.

3.2. Dependence on elevation and relative humidity (RH)

To explore the impact of other parameters on precipitation types, the ANN (Artificial Neural Network) is used to analyze the dependence of the precipitation types on several meteorological and geographic parameters (wind speed, specific humidity, *RH*, air pressure, station elevation, and latitude), and it is found that elevation and *RH* play much more important roles in determining the precipitation types.

To investigate the relationship between elevation and precipitation types, the total elevation range is divided into 6 sub-ranges (0–500, 500–1000, 1000–2000, 2000–3000, 3000–4000, and 4000–5000 m). The sample size of each type (rain, sleet, and snow) in each sub-range is shown in Fig. 2a, and the ratio of each type to the total (within each 0.5 °C bin of T_w) in each elevation sub-range is shown in Fig. 4a–f. It is clearly seen that, along with the increase of elevation, both the bound between snow ratio and sleet ratio and the bound between sleet ratio and rain ratio move toward higher temperature. As a result, a higher temperature threshold is needed for discriminating snow and rain over a higher elevation.

Similarly, the total *RH* range is divided into 5 sub-ranges (0–60%, 60–70%, 70–80%, 80–90%, and 90–100%), and Fig. 4g–k shows the ratio of each precipitation type to total (within each 0.5 °C bin of T_w) in each *RH* sub-range. A striking result is that the probability of sleet occurrence significantly increases with the increase of *RH*.

The dependence of precipitation types on elevation and *RH* can be explained through the energy exchange between precipitation droplets and the ambient air during the falling process. Precipitation droplets generally fall down in a near-surface heating environment, so the precipitation type relies on how many snow droplets can melt away before landing.

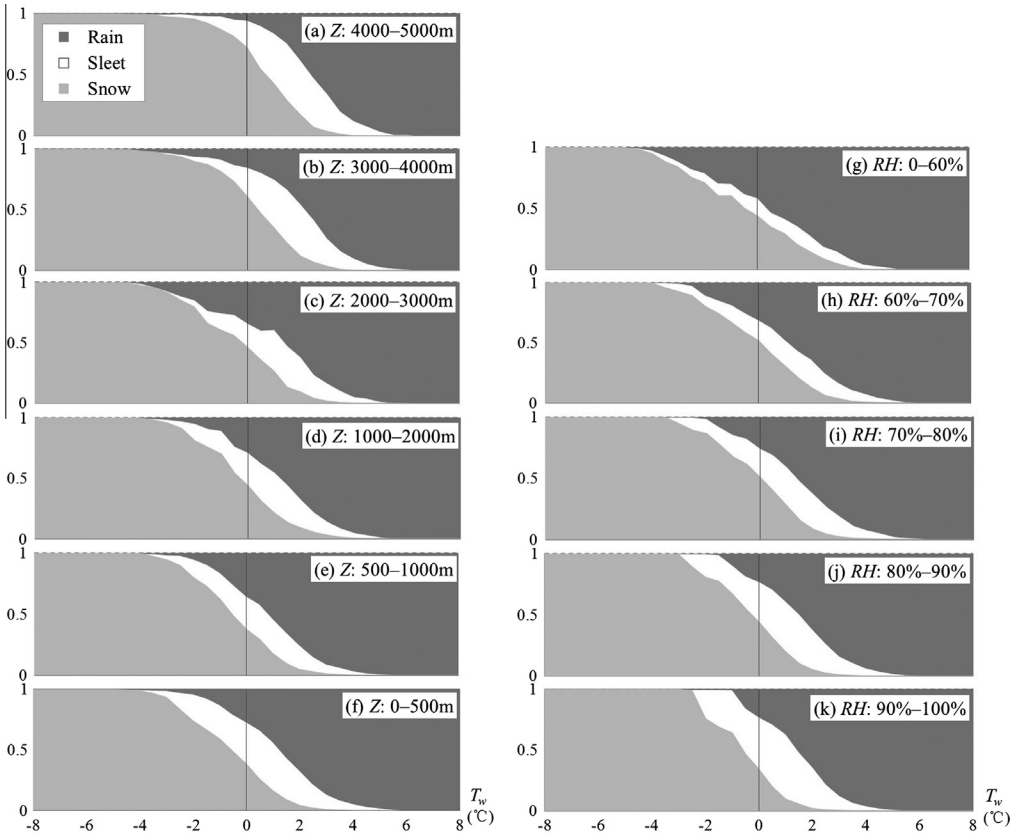

Fig. 4. Similar to Fig. 3, but for each elevation (Z) sub-range (a)–(f) and each relative humidity (RH) sub-range (g)–(k).

A higher elevation implies an environment with lower pressure and thinner air, leading to less drag force on the snow droplets. Thus the droplets can land faster in such an environment, causing the less amount of energy exchanged for melting snow droplets. So the snow droplets tend to keep their original type at a higher elevation. This explains why there is an increasing trend of the temperature threshold for discriminating snow and rain over high-elevation regions (Fig. 4a–f).

Different from the effect of elevation on landing speed of snow droplets, RH mainly affects the speed of the melting process. With the increase of RH, the vapor pressure difference between the surface of the snow droplet and the ambient air decreases, so the evaporation of the droplets becomes slower, and the evaporative cooling effect on the droplets becomes smaller during the falling of the droplets. This is favorable for the transition from snow to rain. Meanwhile, the temperature difference between the snow droplets (close to T_w) and the air (T_a) becomes smaller, so the heat absorbed by the droplets decreases, which may suppress the transition rate of droplets from snow to rain. As a result, the droplets can have a higher probability to appear as sleet in a humid environment than in a dry one (Fig. 4g–k).

4. A new parameterization scheme for precipitation type discrimination

4.1. Parameterizing the occurrence probability of precipitation types

The relationship between the precipitation types and T_w presented in Fig. 4 may be described with three parameters defined in Fig. 5. In Fig. 5, the bound between light grey and white represents the probability of snow (P_1), and the bound between white and dark grey represents the cumulative probability of snow and sleet (P_2). A centralized curve between these two bounds is parameterized by:

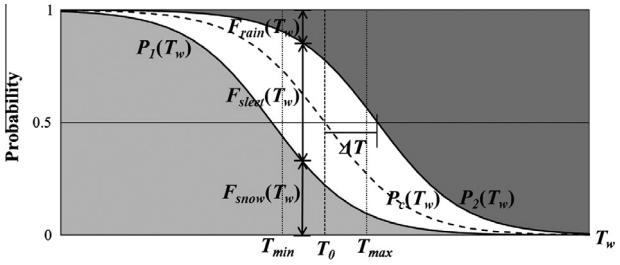

Fig. 5. Sketch map of the relationship between precipitation types and daily mean wet-bulb temperature (T_w). The dark grey, white, and light grey represent the occurrence probabilities of rain (F_{rain}), sleet (F_{sleet}), and snow (F_{snow}) at T_w, respectively. The probability of snow (P_1) and the cumulative probability of snow and sleet (P_2) are denoted by the two solid curves, and $P_c(T_w)$ as the dashed curve is the centralized curve of $P_1(T_w)$ and $P_2(T_w)$. T_{min} and T_{max} are the optimal thresholds of T_w for discriminating snow, sleet, and rain.

$$P_c(T_w) = \frac{1}{1+\exp\left(\frac{T_w - T_0}{\Delta S}\right)}. \quad (1)$$

Then, the P_1–T_w and P_2–T_w relationships can be expressed as:

$$P_1(T_w) = \frac{1}{1+\exp\left(\frac{T_w - T_0 + \Delta T}{\Delta S}\right)}, \quad (2)$$

$$P_2(T_w) = \frac{1}{1+\exp\left(\frac{T_w - T_0 - \Delta T}{\Delta S}\right)}, \quad (3)$$

where T_0, ΔT, and ΔS are parameters to be determined; T_w is the wet-bulb temperature (°C); P_c, P_1, and P_2 all range from 0 to 1.

Once $P_1(T_w)$ and $P_2(T_w)$ are determined, the occurrence probabilities of snow (F_{snow}), sleet (F_{sleet}), and rain (F_{rain}) at T_w can be calculated as:

$$F_{snow}(T_w) = P_1(T_w), \tag{4}$$

$$F_{sleet}(T_w) = P_2(T_w) - P_1(T_w), \tag{5}$$

$$F_{rain}(T_w) = 1 - P_2(T_w). \tag{6}$$

In Eqs. (1)–(3), T_0 is the temperature at which $P_c(T_w)$ is equal to 0.5; it approximately represents the center of T_w range in which snow/rain transition happens. ΔT is the temperature difference between P_c and P_1 (or P_2 and P_c) that gives $P_c = P_1 = P_2 = 0.5$, and $2\Delta T$ shows the temperature range in which sleet mainly occurs. ΔS represents a temperature scale. With the increase of ΔS, the temperature range for snow/rain transition widens. The parameterizations of T_0, ΔT, and ΔS are estimated from the relationship of precipitation types with elevation and *RH* based on the analysis in Section 3.2.

According to the relationship of precipitation types with T_w and elevation (Fig. 4a–f), the three parameters (T_0, ΔT, and ΔS) are obtained in each elevation sub-range. The relationships of the three parameters with the average elevation are shown in Fig. 6a–c. It is seen that T_0 has an overall increasing trend with elevation, while ΔT and ΔS do not have obvious changes with elevation.

Similarly, the three parameters (T_0, ΔT, and ΔS) are obtained from Fig. 4g–k in each *RH* sub-range, and their relationships with the average *RH* are shown in Fig. 6d–f. With the increase of *RH*, an increasing trend in ΔT and a decreasing trend in ΔS are pretty clear. Also, T_0 changes with *RH*.

Since both ΔT and ΔS change with *RH* but not much with elevation, the parameterizations of ΔT and ΔS are developed by their dependences on *RH* and given by:

$$\Delta T = 0.215 - 0.099 \times RH + 1.018 \times RH^2, \tag{7}$$

$$\Delta S = 2.374 - 1.634 \times RH, \tag{8}$$

where *RH* is relative humidity and it ranges from 0 to 1.

As T_0 depends on both elevation and *RH*, it is a function of both elevation and *RH*. Given the values of ΔT and ΔS from Eqs. (7) and (8), the value of T_0 is optimized using the shuffled complex evolution method (Duan et al., 1993) to maximize the accuracy of discriminating the precipitation types. The final result is given by:

$$T_0 = -5.87 - 0.1042 \times Z + 0.0885 \times Z^2 + 16.06 \times RH - 9.614 \times RH^2, \tag{9}$$

where Z denotes station elevation (km).

4.2. A scheme for determinant parameterization of precipitation types

From Eqs. (2)–(9), the occurrence probability of each precipitation type can be calculated by inputting T_w, *RH*, and elevation. For land hydrological modeling, it is usually not sufficient to give the probabilities of the precipitation types; instead, the type for a specific precipitation event must be given. In other words, a determinant identification rather than the probability of a precipitation type is needed. Therefore, two threshold temperatures ($T_{\min}$ and $T_{\max}$) are defined such that the precipitation type is decided by:

$$\text{type} = \begin{cases} \text{snow, if } T_w \leqslant T_{\min}; \\ \text{sleet, if } T_{\min} < T_w < T_{\max}; \\ \text{rain, if } T_w \geqslant T_{\max}. \end{cases} \tag{10}$$

According to the P_1–T_w and P_2–T_w relationships in Fig. 5, $T_{\min}$ is the temperature value at which the occurrence probabilities of snow and sleet are equal to each other, and $T_{\max}$ is that for the equal occurrence probabilities of rain and sleet. These can be expressed as

$$F_{snow}(T_{\min}) = F_{sleet}(T_{\min}), \tag{11}$$

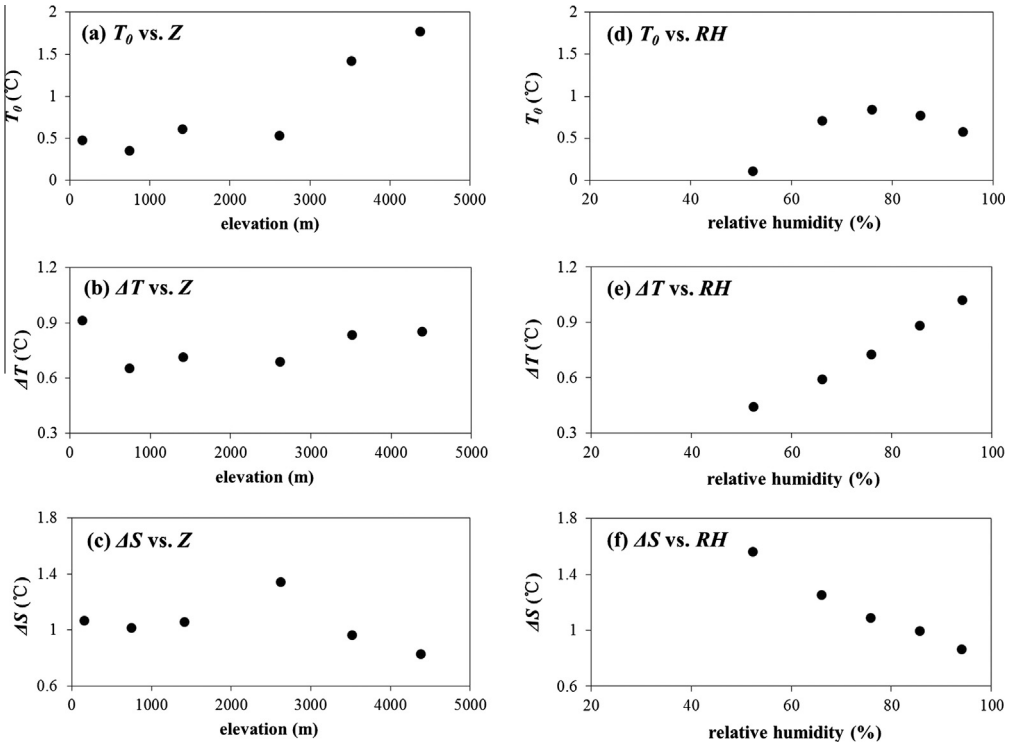

Fig. 6. The relationships of T_0, ΔT, and ΔS with average elevation (Z) in each Z sub-range (a)–(c), and their relationships with average relative humidity (*RH*) in each *RH* sub-range (d)–(f).

$$F_{rain}(T_{\max}) = F_{sleet}(T_{\max}), \quad (12)$$

where F_{snow}, F_{sleet}, and F_{rain} are given by Eqs. (4)–(6).

With the above two equations and Eqs. (2)–(6), the two threshold temperatures can be given below:

$$T_{\min} = \begin{cases} T_0 - \Delta S * \ln\left[\exp\left(\frac{\Delta T}{\Delta S}\right) - 2 * \exp\left(-\frac{\Delta T}{\Delta S}\right)\right] & \frac{\Delta T}{\Delta S} > \ln 2 \\ T_0 & \frac{\Delta T}{\Delta S} \leqslant \ln 2 \end{cases}, \quad (13)$$

$$T_{\max} = \begin{cases} 2 * T_0 - T_{\min} & \frac{\Delta T}{\Delta S} > \ln 2 \\ T_0 & \frac{\Delta T}{\Delta S} \leqslant \ln 2 \end{cases}, \quad (14)$$

where ΔT, ΔS, and T_0 are given by Eqs. (7)–(9).

The deduction of the constraint ($\frac{\Delta T}{\Delta S} > \ln 2$) in the preceding equations is given in the Appendix B. According to Eqs. (7) and (8), the condition of $\frac{\Delta T}{\Delta S} = \ln 2$ is equivalent to $RH = 78\%$. If $RH > 78\%$, $T_{\min}$ and $T_{\max}$ have different values; otherwise, $T_{\min}$ and $T_{\max}$ are identical to each other. In other words, this new parameterization is a dynamic method; it is a dual-threshold method when $RH > 78\%$ and a single threshold method when $RH \leqslant 78\%$. The latter case means that the probability of sleet is so small that it can be ignored when RH is low.

5. Scheme evaluations

The new parameterization scheme developed in Section 4 is evaluated in different regions and periods against the 609 stations in the calibration group and the 100 stations in the validation group (Section 5.1). In addition, all data are used to compare the performance of this scheme with 11 schemes that have already been used in land hydrological models (Section 5.2). The performance is measured by the accuracy of the discrimination of precipitation types over each 0.1 °C bin of T_a.

5.1. Evaluation of the present scheme in different regions and periods

The new scheme is developed based on all calibration data throughout the whole period (1951–1979), and thus, it is important to understand the stability of the performance of the present scheme in different regions and periods.

Fig. 7a presents the performance of the new scheme in the mainland of China, three main snowfall regions of China (the Tibetan Plateau (TP), Northwest China (NW), Northeast China (NE)), and the rest of China (Rest) for the whole period. The white bars denote the discrimination accuracy for the calibration group, and the black ones denote that for the validation group. Against the calibration group, the average accuracy of this scheme for the mainland of China exceeds 88% over [−10 °C, 10 °C] of T_a. Furthermore, its accuracy exceeds 86% for all the four sub-regions. It can be seen that the accuracy over the TP is slightly higher than the other three sub-regions, which implicates a better performance of the scheme in highland regions.

In order to investigate the time stability of the present scheme, the whole study period is divided into three sub-periods: 1951–1960, 1961–1970, and 1971–1979. The white bars in Fig. 7b show the performance of the present scheme in each sub-period over the T_a range [−10 °C, 10 °C]. The accuracy of the scheme is about 88% for the whole period, and it is quite stable for the three sub-periods, indicating that the new scheme has a robust performance.

The performance of the new scheme against the independent validation data is very close to and even slightly better than the one against the calibration data, as shown in Fig. 7. This further proves the general applicability of the present scheme in China.

5.2. Scheme inter-comparisons

A number of schemes for precipitation-type discrimination have been used in land hydrological models, and this section presents the performances of 11 schemes in the literature in comparison with the present scheme. Table 1 lists the 11 schemes in the literature. Among them, nine schemes are used for precipitation-type classification: Y97 is a single threshold method; L93, W94,

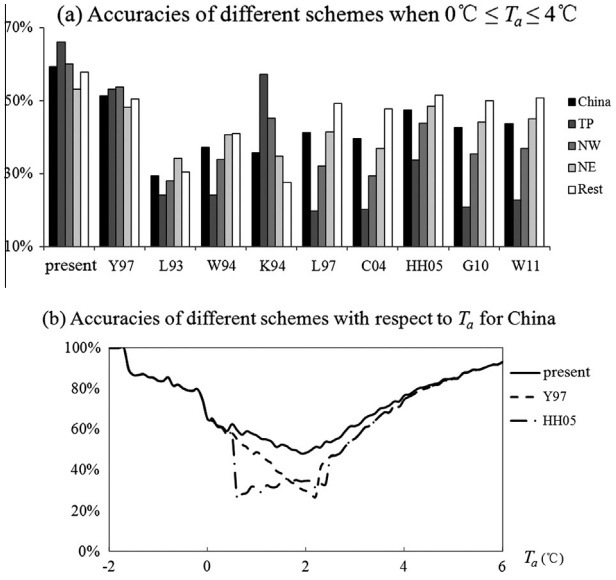

Fig. 8. (a) Accuracy of the present scheme and nine threshold schemes (first nine in Table 1) over the air temperature range [0 °C, 4 °C] in China, the Tibetan Plateau (TP), Northwest China (NW), Northeast China (NE), and the rest of China (Rest), respectively. (b) Air temperature-dependence of the accuracy of the present scheme, Y97 scheme, and HH05 scheme for China.

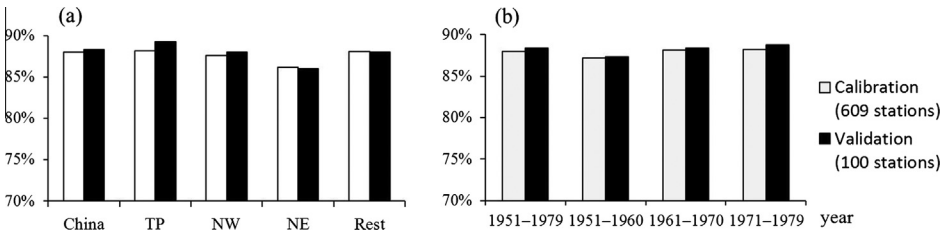

Fig. 7. The accuracies of the present scheme in different regions and periods over the air temperature range [−10 °C, 10 °C]. (a) The spatial evaluation for China, the Tibetan Plateau (TP), Northwest China (NW), Northeast China (NE), and the rest of China (Rest); (b) the temporal stability of the accuracy for different periods (the whole period and the periods of 1951–1960, 1961–1970, and 1971–1979). The white bars denote the accuracy of the precipitation-type discrimination based on the 609 calibration stations, and the black ones for the 100 validation stations.

Table 2
Accuracies of the precipitation-type discrimination of the present scheme and nine schemes in the literature over the air temperature range [0 °C, 4 °C].

	Present (%)	Y97 (%)	L93 (%)	W94 (%)	K94 (%)	L97 (%)	C04 (%)	HH05 (%)	G10 (%)	W11 (%)
China	59.3	51.4	29.4	37.2	35.7	41.3	39.6	47.4	42.6	43.7
TP	66.1	53.2	24.1	24.1	57.2	19.7	20.3	33.8	20.9	22.8
NW	60.1	53.8	28.1	34.0	45.3	32.2	29.4	43.9	35.5	37.0
NE	53.1	48.3	34.3	40.6	34.8	41.5	36.9	48.4	44.1	45.1
Rest	57.8	50.5	30.4	40.9	27.5	49.3	47.8	51.6	50.0	50.7

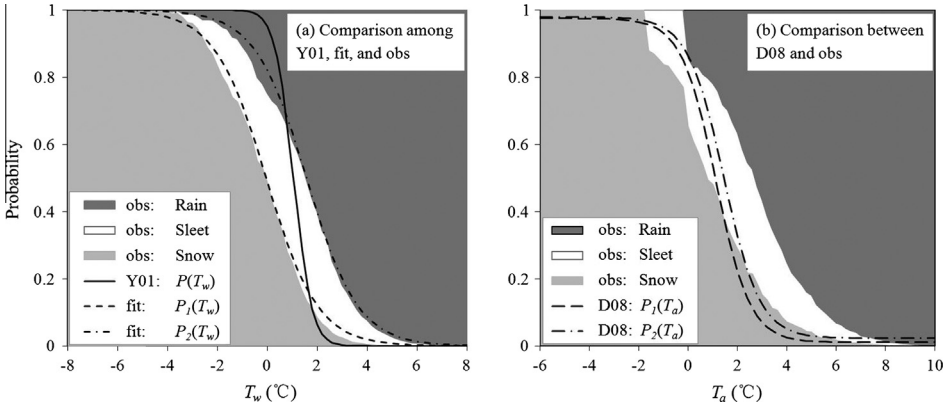

Fig. 9. (a) The P_1–T_w and P_2–T_w relationships from observed data (obs), their fitted curves (fit) according to Eqs. (2) and (3), and the P–T_w relationship (P is the ratio of snow amount to total precipitation amount) given by Y01 scheme; (b) the P_1–T_a and P_2–T_a relationships between the observed and D08 scheme.

K94, L97, C04, HH05, G10, and W11 are dual-threshold methods. Other two schemes (Y01 and D08) are used to calculate the ratio of snow (or rain) amount to total precipitation amount with input of T_w or T_a. The specific temperature thresholds to discriminate precipitation types or the variable used to estimate the snow ratio for these schemes are summarized in Table 1.

Fig. 8a compares the accuracy between the present scheme and the nine threshold schemes (the first nine schemes in Table 1) over the T_a range [0 °C, 4 °C] in China and the four sub-regions of China (TP, NW, NE, and Rest). It is seen that the accuracy of all schemes for the [0 °C, 4 °C] range is worse than that for the [−10 °C, 10 °C] range (Fig. 7), indicating that the discrimination of precipitation types for the [0 °C, 4 °C] range is more difficult. Perhaps, precipitation types over this temperature range are more sensitive to ambient air conditions. Nevertheless, the accuracy of the present scheme is clearly better than that of the nine schemes for the whole region and each of the four sub-regions, as also indicated in Table 2. Among the nine schemes, Y97 scheme shows better performance in the four sub-regions; K94 scheme also has good performance for TP and NW but not so for NE and Rest, perhaps because K94 scheme is obtained from high-elevation observations; other seven schemes generally perform better for the low-elevation regions than the high-elevation regions, perhaps because they focus more on low-elevation regions or estimate the threshold temperatures by experiences. In turn, this demonstrates the dependence of precipitation types on elevation. The difference in the accuracy between the present scheme and Y97 scheme is nearly 7.9% for China (59.3% and 51.4% for the two schemes, respectively), 12.9% for TP (66.1% and 53.2%, respectively), 6.3% for NW (60.1% and 53.8%, respectively), 4.8% for NE (53.1% and 48.3%, respectively), and 7.3% for Rest (57.8% and 50.5%, respectively), as shown in Fig. 8a. The accuracy difference between the present scheme (66.1%) and K94 scheme (57.2%) for TP is nearly 8.9%, and that between the present scheme (57.8%) and HH05 scheme (51.6%, the best one among the nine schemes) for Rest is about 6.2%. To show the performance of the present scheme more clearly, Fig. 8b compares the accuracy distribution of this scheme with Y97 scheme and HH05 scheme (the best two schemes among the nine) with respect to T_a for China. Again, it can be seen that the present scheme performs better at any specific T_a value.

Fig. 9a shows the comparison of P_1–T_w and P_2–T_w relationships from the observed data, the fitted curves (i.e. Eqs. (2) and (3)), and Y01 scheme. It is noticed that Y01 scheme only gives the estimates of snow (F_{snow}) and rain ratio (F_{rain}), while the observed data and the fitted curves give snow (F_{snow}), sleet (F_{sleet}), and rain ratio (F_{rain}). Although they cannot be compared directly by values, it can be seen that Y01 scheme underestimates the rain ratio when T_w is below 1 °C and overestimates the rain ratio when T_w is above 2 °C. Fig. 9b compares the P_1–T_a and P_2–T_a relationships between observed data and D08 scheme. It seems that D08 scheme underestimates the sleet ratio.

In summary, the present scheme is based on a long-term dataset with different climate regimes and elevation regions, and it generally performs better than other schemes in the literature.

6. Conclusion and remarks

Precipitation type is an important input for the study of land hydrological processes, and usually determined by static temperature thresholds in most current hydrological models. To better discriminate rain, sleet, and snow, this study presented the relationships of precipitation types with elevation and meteorological variables based on CMA station data during 1951–1979, and then a new parameterization scheme was developed.

It is found that wet-bulb temperature is a better indicator of precipitation types than air temperature although the latter is more widely used in discriminating precipitation types. Precipitation types are also highly dependent on elevation and humidity. Over higher-elevation regions, snow droplets can land faster and thus absorb less heat from the ambient air. So the droplets tend to stay as snow at high elevations and a higher threshold temperature is needed for discriminating snow and rain. In a humid environment, small humidity difference between droplets and ambient air leads to small evaporative cooling and thus is favorable for the phase transition from snow to rain, but the intensity of the

transition is suppressed by the small heat transfer from the air to the snow droplets, resulting in more sleet.

Based on these findings, a new parameterization scheme was developed to discriminate rain, sleet, and snow. In this scheme, the threshold temperatures dynamically change with humidity and elevation. The dynamic threshold method tends to be a dual-threshold method in a humid environment and a single threshold method in a dry environment. Several evaluations show consistent good performance of the new scheme in different regions and periods, and also indicate that the new scheme performs better than other schemes in the literature.

Finally, it is worthy to note that the scheme was only evaluated for China territory, and further evaluations for other regions are needed. Furthermore, the new scheme was developed based on daily meteorological data, and thus it may be different from schemes developed based on hourly data. As the temperature during precipitation hours is usually lower than the daily mean temperature, the threshold temperature needed for identifying hourly precipitation types is expected to be lower than the values given by the present scheme.

Acknowledgments

This research was financially supported by the Strategic Priority Research Program (B) of the Chinese Academy of Sciences (Grant No. XDB03030300) and the National Natural Science Foundation of China (Grant Nos. 41190083 and 41325019). The meteorological data used in this study were provided by CMA National Meteorological Information Center. The authors thank the anonymous reviewers for their valuable comments.

Appendix A. Wet-bulb temperature (T_w)

T_w is the temperature of a parcel of saturated air if the saturation is due to evaporation into it, with the latent heat supplied by the parcel itself. This process can be expressed as:

$$c_p(T_a - T_w) + \frac{\varepsilon L_v}{p_s}(e_a - e_{w,sat}) = 0, \tag{A.1}$$

where $c_p = 1004\ \mathrm{J\ K^{-1}\ kg^{-1}}$, $\varepsilon = 0.622$, $L_v = 2.5104 \times 10^6\ \mathrm{J\ kg^{-1}}$, p_s is air pressure [h Pa], T_a is air temperature [°C], T_w is wet-bulb temperature [°C], e_a is vapor pressure [h Pa], and $e_{w,sat}$ is the saturated vapor pressure [h Pa] at T_w.

From the above equation, T_w can be deduced as:

$$T_w = T_a - \frac{e_{sat}(T_a)(1 - RH)}{0.000643 p_s + \frac{\partial e_{sat}}{\partial T_a}}, \tag{A.2}$$

where RH is relative humidity and it ranges from 0 to 1; $e_{sat}(T_a)$ is the saturated vapor pressure [h Pa] at T_a and is given by Tetens's empirical formula (Murray, 1967) as:

$$e_{sat}(T_a) = 6.1078 \exp\left(\frac{17.27 T_a}{T_a + 237.3}\right). \tag{A.3}$$

Appendix B. Deduction of the constraint for the optimal threshold temperatures

There are two constraints for Eqs. (13) and (14), as given below:

$$\exp\left(\frac{\Delta T}{\Delta S}\right) - 2 * \exp\left(-\frac{\Delta T}{\Delta S}\right) > 0, \tag{B.1}$$

and

$$T_{\min} < T_{\max}, \tag{B.2}$$

in which, Eq. (B.1) is a constraint required by the logarithmic term in Eq. (13), and Eq. (B.2) is a physical constraint.

Putting Eqs. (13) and (14) into Eq. (B.2), we have

$$\Delta S * \ln\left[\exp\left(\frac{\Delta T}{\Delta S}\right) - 2 * \exp\left(-\frac{\Delta T}{\Delta S}\right)\right] > 0, \tag{B.3}$$

where ΔS is a function of RH (Eq. (8)) and gives a value consistently larger than 0 over the RH range [0, 1]. So Eq. (B.3) is equivalent to

$$\exp\left(\frac{\Delta T}{\Delta S}\right) - 2 * \exp\left(-\frac{\Delta T}{\Delta S}\right) > 1, \tag{B.4}$$

which also satisfies Eq. (B.1).

Eq. (B.4) can eventually be simplified as:

$$\frac{\Delta T}{\Delta S} > \ln 2, \tag{B.5}$$

which is the constraint for Eqs. (13) and (14).

References

Anderson, B., Mackintosh, A., 2012. Controls on mass balance sensitivity of maritime glaciers in the Southern Alps, New Zealand: the role of debris cover. J. Geophys. Res. Earth Surf. 117, F01003, <http://dx.doi.org/10.1029/2011JF002064>.

Auer Jr., A.H., 1974. The rain versus snow threshold temperatures. Weatherwise 27, 67, <http://dx.doi.org/10.1080/00431672.1974.9931684>.

Benjamin, S.G., Grell, G.A., Brown, J.M., Brundage, K.J., Devenyi, D., Kim, D., Schwartz, B., Smirnova, T.G., Smith, T.L., Weygandt, S.S., 2000. The 20-km version of the Rapid Update Cycle. In: 9th Conf. on Aviation, Range, and Aerospace Meteorology, pp. 421–423.

Bocchieri, J.R., 1980. The objective use of upper air soundings to specify precipitation type. Mon. Weather Rev. 108, 596–603.

Bourgouin, P., 2000. A method to determine precipitation types. Weather Forecasting 15, 583–592.

Box, J., Fettweis, X., Stroeve, J., Tedesco, M., Hall, D., Steffen, K., 2012. Greenland ice sheet albedo feedback: thermodynamics and atmospheric drivers. Cryosphere 6, 821–839, <http://dx.doi.org/10.5194/tc-6-821-2012>.

Chen, R.S., Lu, S.H., Kang, E.S., Ji, X.B., Zhang, Z., Yang, Y., Qing, W., 2008. A distributed water-heat coupled model for mountainous watershed of an inland river basin of Northwest China (I) model structure and equations. Environ. Geol. 53, 1299–1309, <http://dx.doi.org/10.1007/s00254-007-0738-2>.

Clark, M.P., Slater, A.G., Barrett, A.P., Hay, L.E., McCabe, G.J., Rajagopalan, B., Leavesley, G.H., 2006. Assimilation of snow covered area information into hydrologic and land-surface models. Adv. Water Resour. 29, 1209–1221, <http://dx.doi.org/10.1016/j.advwatres.2005.10.001>.

Collins, W.D., Rasch, P.J., Boville, B.A., Hack, J.J., McCaa, J.R., Williamson, D.L., Kiehl, J.T., Briegleb, B., Bitz, C., Lin, S.J., Zhang, M.H., Dai, Y.J., 2004. Description of the NCAR community atmosphere model (CAM 3.0). NCAR Tech. Note NCAR/TN-464+ STR.

Czys, R.R., Scott, R.W., Tang, K.C., Przybylinski, R.W., Sabones, M.E., 1996. A physically based, nondimensional parameter for discriminating between locations of freezing rain and ice pellets. Weather Forecasting 11, 591–598.

Dai, A.G., 2008. Temperature and pressure dependence of the rain-snow phase transition over land and ocean. Geophys. Res. Lett. 35, L12802, <http://dx.doi.org/10.1029/2008GL033295>.

Duan, Q.Y., Gupta, V.K., Sorooshian, S., 1993. Shuffled complex evolution approach for effective and efficient global minimization. J. Optim. Theory Appl. 76, 501–521.

Gao, X., Ye, B.S., Zhang, S.Q., Qiao, C.J., Zhang, X.W., 2010. Glacier runoff variation and its influence on river runoff during 1961–2006 in the Tarim River Basin, China. Sci. China Earth Sci. 53, 880–891, <http://dx.doi.org/10.1007/s11430-010-0073-4>.

Gustafsson, D., Stähli, M., Jansson, P.E., 2001. The surface energy balance of a snow cover: comparing measurements to two different simulation models. Theor. Appl. Climatol. 70, 81–96.

Han, C.T., Chen, R.S., Liu, J.F., Yang, Y., Qing, W.W., 2010. A discuss of the separating solid and liquid precipitations. J. Glaciol. Geocryol. 32, 249–256 (in Chinese).

Hock, R., Holmgren, B., 2005. A distributed surface energy-balance model for complex topography and its application to Storglaciaren, Sweden. J. Glaciol. 51, 25–36.

Kang, E.S., 1994. Energy, water and mass balance, and discharge modeling in the Tianshan glaciated basin. Sci. China. Ser. B 24, 983–991 (in Chinese).

Kang, E.S., Cheng, G.D., Lan, Y.C., Jin, H.J., 1999. A model for simulating the response of runoff from the mountainous watersheds of inland river basins in the arid area of northwest China to climatic changes. Sci. China Ser. D: Earth Sci. 42, 52–63.

Lindström, G., Johansson, B., Persson, M., Gardelin, M., Bergström, S., 1997. Development and test of the distributed HBV-96 hydrological model. J. Hydrol. 201, 272–288.

Loth, B., Graf, H.F., Oberhuber, J.M., 1993. Snow cover model for global climate simulations. J. Geophys. Res. Atmos. (1984–2012) 98, 10451–10464.

Lundquist, J.D., Neiman, P.J., Martner, B., White, A.B., Gottas, D.J., Ralph, F.M., 2008. Rain versus snow in the Sierra Nevada, California: comparing Doppler profiling radar and surface observations of melting level. J. Hydrometeorol. 9, 194–211, <http://dx.doi.org/10.1175/2007JHM853.1>.

Murray, F.W., 1967. On the computation of saturation vapor pressure. J. Appl. Meteorol. 6, 203–204.

Rasmussen, R., Baker, B., Kochendorfer, J., Meyers, T., Landolt, S., Fischer, A.P., Black, J., Thériault, J.M., Kucera, P., Gochis, D., Smith, C., Nitu, R., Hall, M., Ikeda, K., Gutmann, E., 2012. How well are we measuring snow: the NOAA/FAA/NCAR winter precipitation test bed. Bull. Amer. Meteorol. Soc. 93, 811–829, <http://dx.doi.org/10.1175/BAMS-D-11-00052.1>.

Rauber, R.M., Olthoff, L.S., Ramamurthy, M.K., Kunkel, K.E., 2001. Further investigation of a physically based, nondimensional parameter for discriminating between locations of freezing rain and ice pellets. Weather Forecasting 16, 185–191.

Ryzhkov, A.V., Zrnic, D.S., 1998. Discrimination between rain and snow with a polarimetric radar. J. Appl. Meteorol. 37, 1228–1240.

Schuur, T.J., Park, H.S., Ryzhkov, A.V., Reeves, H.D., 2012. Classification of precipitation types during transitional winter weather using the RUC model and polarimetric radar retrievals. J. Appl. Meteor. Climatol. 51, 763–779, <http://dx.doi.org/10.1175/JAMC-D-11-091.1>.

Wang, S., Pu, J.C., Wang, N.L., 2011. Study of mass balance and sensibility to climate change of qiyi glacier in qilian mountains. J. Glaciol. Geocryol. 33, 1214–1221 (in Chinese).

Wigmosta, M.S., Vail, L.W., Lettenmaier, D.P., 1994. A distributed hydrology-vegetation model for complex terrain. Water Resour. Res. 30, 1665–1679.

Yamazaki, T., 2001. A one-dimensional land surface model adaptable to intensely cold regions and its applications in Eastern Siberia. J. Meteor. Soc. Japan 79, 1107–1118.

Yang, D.Q., Jiang, T., Zhang, Y.S., Kang, E.S., 1988. Analysis and correction of errors in precipitation measurement at the head of Urumqi River. Tianshan. J. Glaciol. Geocryol. 10, 384–399 (in Chinese).

Yang, D.Q., Goodison, B.E., Metcalfe, J.R., Golubev, V.S., Elomaa, E., Gunther, T., Bates, R., Pangburn, T., Hanson, C.L., Emerson, D., Copaciu, V., Milkovic, J., 1995. Accuracy of Tretyakov precipitation gauge: result of WMO intercomparison. Hydrol. Process. 9, 877–895.

Yang, Z.L., Dickinson, R.E., Robock, A., Vinnikov, K.Y., 1997. Validation of the snow submodel of the biosphere-atmosphere transfer scheme with Russian snow cover and meteorological observational data. J. Climate 10, 353–373.

Zhang, G.S., Kang, S.C., Fujita, K., Huintjes, E., Xu, J.Q., Yamazaki, T., Haginoya, S., Yang, W., Scherer, D., Schneider, C., Yao, T.D., 2013. Energy and mass balance of Zhadang glacier surface, central Tibetan Plateau. J. Glaciol. 59, 137–148, <http://dx.doi.org/10.3189/2013JoG12J152>.